International Journal of Disaster Risk Reduction 82 (2022) 103325

Contents lists available at ScienceDirect

International Journal of Disaster Risk Reduction

journal homepage: www.elsevier.com/locate/ijdrr

A novel approach of multi-hazard integrated zonation on the ancient Silk Road

Qiang Zou [a, b, *], Peng Cui [a, b, d, **], Zhengtao Zhang [c], Koert Sijimons [e], Giacomo Titti [f], Shusong Li [a], Hu Jiang [a]

[a] Key Laboratory of Mountain Hazards and Earth Surface Process/Institute of Mountain Hazards and Environment, Chinese Academy of Sciences (CAS), Chengdu, China
[b] China-Pakistan Joint Research Center on Earth Sciences, CAS-HEC, Islamabad, Pakistan
[c] Beijing Normal University, Beijing, China
[d] Institute of Geographical Science and Resources, Chinese Academy of Sciences (CAS), Beijing, China
[e] Institute of Earth Information Science and Earth Observation, Twente University, Twente, Netherlands
[f] Research Institute for Geo-Hydrological Protection, National Research Council, Padova, Italy

ARTICLE INFO

Keywords:
Natural hazards
Geomorphology
Climate
Hazard-causing mechanism
Silk road

ABSTRACT

Hazard identification is crucial for disaster risk reduction in areas featuring multiple co-occurring hazards and active internal and external dynamic geographical processes. Coupling the elements of external hazard-forming environments and the internal mechanisms inducing hazards, a novel multi-hazard integration zonation (MIZ) method has been developed in which a segmented multi-hazard identification function was constructed to identify the dominant hazard types and their boundaries in a region. Taking the ancient Silk Road as a case study, the major types and spatial zonation of multiple hazards have been identified, which are in accordance with the actual disaster situation. These sympatric multiple hazards present a widely spatial scattered distribution of individual hazards and a more concentrated distribution of multiple hazards in the ancient Silk Road area. These results, combined with the geomorphological features and the climatic zones of the analyzed area, reveal the spatial boundaries among these major hazards at the macro- and microscales. These findings suggest that the proposed MIZ methodology can provide scientific support for rational engineering layouts and regional planning and may serve as pertinent guidance for multi-hazard identification in ancient Silk Road area and beyond.

1. Introduction

The ancient Silk Road originated in 207 B.C. and has lasted for more than two thousand years serving as a complex network that connects China with the trade centers of the eastern Mediterranean and other regions [1,2]. The Silk Road region covers more than 100 countries that encompass nearly 66% of the world's population [3,4]. The Silk Road has long played a significant role in the global exchange of economic resources, trade, science, technology, and civilization. However, due to the complex geological and geomorphological environments, the increase in natural hazards in recent decades has challenged to the social and economic development of the countries in this region [5–7]. Furthermore, such hazards can significantly hinder the sustainable development of Silk

* Corresponding author. Key Laboratory of Mountain Hazards and Earth Surface Process/Institute of Mountain Hazards and Environment, Chinese Academy of Sciences (CAS), Chengdu, China.
** Corresponding author. China-Pakistan Joint Research Center on Earth Sciences, CAS-HEC, Islamabad, Pakistan.
E-mail addresses: zouqiang@imde.ac.cn (Q. Zou), pengcui@imde.ac.cn (P. Cui).

https://doi.org/10.1016/j.ijdrr.2022.103325
Received 29 April 2022; Received in revised form 19 September 2022; Accepted 22 September 2022
Available online 29 September 2022

Road countries if the hazards are not well studied and understood for the best interests of all mankind. In coherence with the Sendai Framework for Disaster Risk Reduction 2015–2030 (SFDRR) and the UN 2030 Sustainable Development Goals (SDGs), it is of primary importance to comprehensively investigate and identify the main natural hazards and their spatial distributions in this region, especially when multiple hazards coincide in the same area.

Hazard identification is a critical fundament for disaster risk reduction and hazard mitigation decision-making [8]. In recent decades, the spatial distribution of natural hazards has been identified by focusing on hazard-forming factors, hazard distribution and hazard severity. Based on historical data or the interpretation from remote sensing and aerial photography, the spatial distribution of hazard-forming factors can be identified. Additionally, the hazard severity can be further calculated using qualitative or quantitative methods and GIS technology. Most qualitative methods have focused on identifying the spatial distribution directly on the basis of visual interpretation and experience-based judgment [9,10]. In contrast, quantitative methods are based on statistical principles, such as the weighted synthesis method [11–13] combined with remote sensing and GIS technology [14,15], artificial neural network methods [16,17] or a hazard threshold [18]. According to the characteristics of natural hazards, this research attempts objectively determine the effects of individual factors on hazard formation and then identify the hazard severity distribution by overlaying each hazard-forming element. Through the analysis of the geological and geomorphological environment and climatic conditions, the spatial distribution of hazards can be determined with the multifactor analysis method. For instance, the spatial distribution of hazard severity can be estimated by analyzing the hazard or susceptibility of the geomorphological map [19,20] or building models consistent with the hazard-forming mechanism [21]. Moreover, a more comprehensive hazard severity evaluation of multiple hazards can be obtained by integrating the severity distribution of each natural hazard, and the results can be further analyzed to reveal the distribution pattern of the integrated hazard severity in different zones. To date, some scientists have conducted research on multi-hazard assessment and mapping. Numerous theoretical approaches and empirical methods have been developed for determining the spatial distribution and severity of individual and multiple hazards [22,23,59]; Tuhin Ghosh, 2014). Moreover, considering the compound and chain-reaction effects of multiple hazards, different methods have recently been proposed for producing multi-hazard maps, including a synthetic-hazard map, aggregate-hazard map, stability map, suitability map and accumulated risk map [10,24,25,60]. However, the lacks of an effective method for comprehensively combining the spatial distribution of multiple hazards and a well-defined method for determining the boundaries of multiple hazards limit the ability to identify major hazards.

To scientifically and quantitatively determine the spatial zone for the multiple hazards that occur in the countries and regions along the ancient Silk Road, this study intends to create a novel multi-hazard integrated zonation (MIZ) method that combines the elements of external hazard-forming environments with the internal mechanisms inducing hazards.

2. Methodology

2.1. Multi-hazard integrated zonation (MIZ) method

Different types of natural hazards frequently occur along the ancient Silk Road, and multiple hazards repeatedly appear in the same regions. Thus, identifying the main hazards and the boundaries of each hazard is essential to constructing the MIZ method. Through the analysis of hazard-causing mechanisms and hazard-forming environments, a segmented function for multi-hazard identification was built. Accordingly, a zonation method was proposed based on the distribution of hazard severity and the spatial distribution of landforms and climate zones.

To identify the main types of hazards, the segmented function of multi-hazard identification is established based on the spatial distribution of each hazard severity, and the formula is as follows:

$$Y^R = \begin{cases} \max\limits_{1\le i\le n}\{D_i\}, & D_i \neq D_j\,(1 \le i \neq j \le n) \\ D_1 \& D_2 \cdots \& D_i, & D_i = D_j\,(1 \le i \neq j \le n) \end{cases} \tag{1}$$

where $Y^R$is the main hazard type in region R, i represents the number of hazard types (up to n), and D_i represents the severity of the i^{th} type of hazard in region R.

The segmented function can be developed by considering the following three different circumstances.

- If there is only one type of hazard in region R, it is the main hazard type, and its severity is D_i.
- If multiple hazards occur simultaneously in a region and their severities are quite different, the main hazard type is the one with the highest severity in the area, and its severity is equal to $Max(D_1 \ \& \ D_2 \ \ldots \ \& D_i)$.
- If multiple hazards occur simultaneously in a region and two or more of the hazards feature severities that are both similar and the highest in the area, the results are multiple types of natural hazards with the highest severity of $D_1 \& D_2 \cdots \& D_i$ in the study area, and the severity is D_i.

To identify the spatial boundaries of multiple hazards, different types of hazards and their external hazard-forming environments should be comprehensively analyzed. And a schematic diagram is shown in Fig. 1. Specifically, the vertical part I in Fig. 1 shows that the zoning of hazard-forming environments is tangential to or separated from the boundaries of hazard severity. There is no spatially overlapping relationship between them; therefore, the determined hazard zone still follows the original boundary of the hazard severity. The vertical part II in Fig. 1 shows the spatially overlapping relationship between the hazard severity and the hazard-forming environment. The overlapping relationship can be further considered in the following two situations. (a) If the hazard-forming environment condition in the overlapping area highly contributes to the formation processes of the hazard type in the hazard severity area, the hazard zone will be jointly based on the boundary of the hazard severity and the hazard-forming environment. (b) If the overlap-

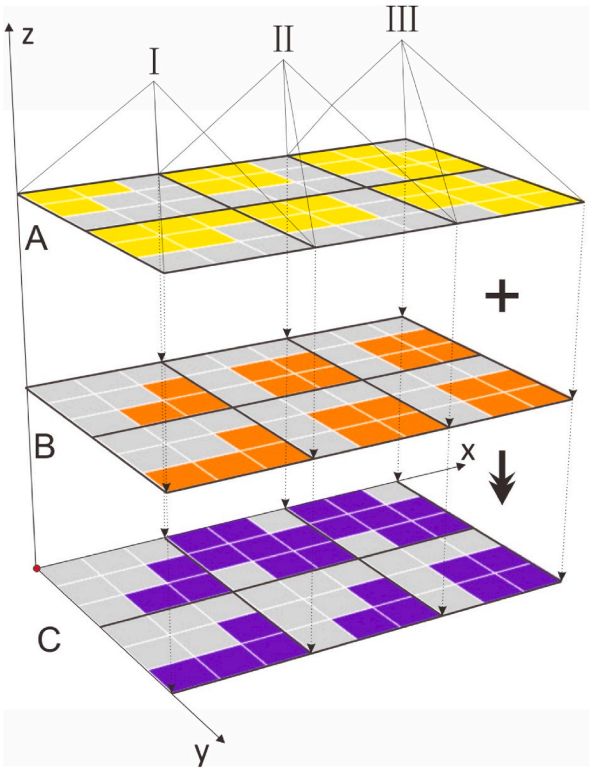

Fig. 1. The schematic diagram of boundary identification of multiple hazards (Layer A is the zoning of hazard-forming environments; Layer B is the spatial distribution of hazard severity; Layer C represents the spatial boundary result for multiple hazards).

ping part is not conducive to hazard formation, the hazard zone needs to exclude the overlapping area. The vertical part III in Fig. 1 shows the spatially inclusive relationship between the hazard severity and the hazard-forming environment. If the hazard-forming environment is conducive to forming the corresponding hazard, the final hazard zone will expand to the boundary of the environmental zone. Otherwise, the final hazard zone will still be determined by the original boundaries of the hazard severity.

According to this MIZ approach, the major natural hazards and their integrated zonation can be determined by using GIS techniques. The flowchart of the method is shown in Fig. 2. Two crucial issues have been analyzed in the MIZ method: (a) The external environments mainly refer to the geomorphological characteristics and climatic zones that are conducive to the formation of natural hazards, (b) The internal hazard mechanisms and characteristics which determines different spatial distributions of natural hazards.

2.2. Method of geomorphology classification

The frequency of different natural hazards is closely related to the differentiation patterns of the geomorphological conditions along the ancient Silk Road. Spatial geomorphological landforms are shaped by the internal geological tectonic activity and the external influences of flowing water, wind, atmosphere and biology. These landscapes present three-dimensional continuity, a high degree of diversity and exhibit spatial proximity. To quantitatively demarcate the ancient Silk Road geomorphological characteristics, the geomorphological classification principle and criteria have been adopted as references [26–29], and the elevation and the elevation difference have been selected as the two fundamental factors in the geomorphology classification.

The differences among complex geomorphologic units, their geomophogensis and the scale of the diverse landforms should be considered. In this article, plains, plateaus and mountains are initially classified based on regional elevation and terrain characteristics. Then, the mountains are further subdivided with land surface relief. Table 1 shows the classification of the geomorphic types. This method objectively illustrates the activity and intensity of plate tectonic evolution, which is physically and mechanically related to the spatial distribution of earthquakes, geological hazards and tsunamis.

2.3. Climate zoning

The multiple natural hazards along the ancient Silk Road are closely related not only to geomorphological conditions but also to atmospheric circulation conditions. The spatial differences in the precipitation and temperature levels provide the conditions necessary to form floods, freezing events and ocean hazards. Due to global climate change, the aggravation of extreme weather and climate events has become a key factor in the formation of natural hazards [30,31]. Therefore, on the basis of topographic and geomorphic zonation, climate zoning can further reasonably define the boundaries of hazard-forming environments. In this study, through using the GIS spatial analysis technology, the latest map of climate classifications is drawn based on a recent data set from the Climatic Research Center (CRU) of the University of East Anglia and the Global Precipitation and Climatology Center (GPCC) of the German Me-

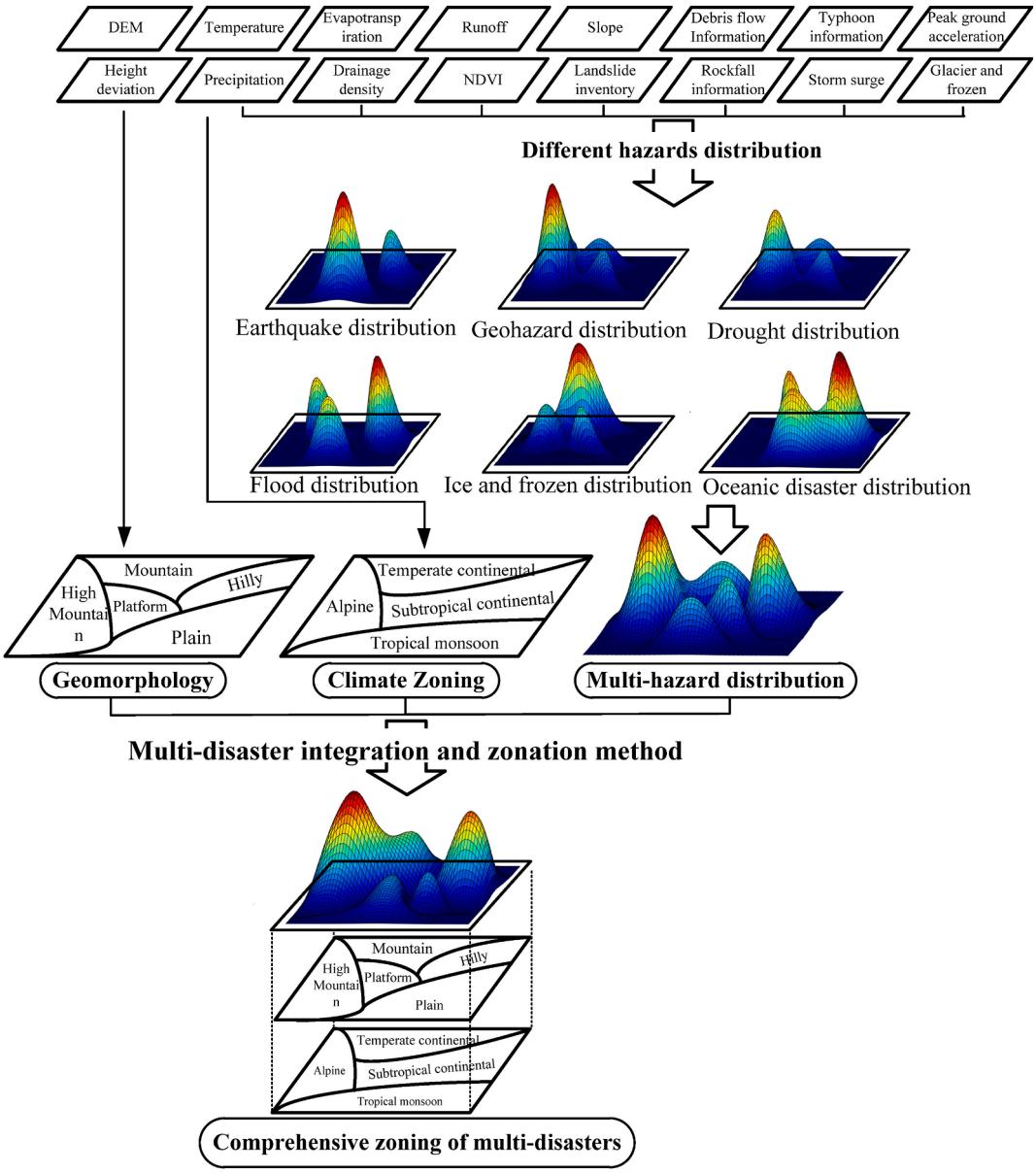

Fig. 2. Flowchart of the multi-hazard integrated zonation (MIZ) method.

teorological Office. This map from GPCC is an international research result and can consistent with the current global climate characteristics, as well as has been relatively widely used in disaster risk research [32].

2.4. Method for determining different hazard distributions

By analyzing the different distributions and spatial forms of natural hazards, the spatial distribution characteristics of various types of natural hazards in the study area can be described. As specific examples, earthquakes, droughts, floods, freezing events and ocean hazards are selected as typical hazards to introduce the hazard distribution method.

2.4.1. Earthquakes

To evaluate the intensity of ground motion or earthquake hazards, scholars have developed different scientific parameters, including the Arias intensity (I_A), cumulative absolute velocity (CAV) and frequency content indicators [33–36,61]. In this study, the value of peak ground acceleration (PGA), which is often determined by the maximum value of the seismic pulse, is used to characterize earthquake intensity. The magnitude of PGA in the horizontal direction on the earth surface can be calculated based on analyzing the seismic tectonic environment, historical seismicity, attenuation in the spread of seismic ground motion generated in earthquakes above magnitude 4.0, and near-surface site conditions [37].

Table 1
Landform types and parameters of the geomorphological classification.

Landform types	Elevation	Low elevation (<1000 m a.s.l.)	Medium elevation (1000–2000 m a.s.l.)	Medium-high elevation (2000–4000 m a.s.l.)	High elevation (4000–6000 m a.s.l.)	Extremely high elevation (>6000 m a.s.l.)
Plain	Plain (<30 m)	Low-elevation plain	Medium-elevation plain	Medium-high-elevation plain	High-elevation plain	–
Plateau	Plateau (30–100 m)	Low-elevation plateau	Medium-elevation plateau	Medium-high-elevation plateau	High-elevation plateau	–
Mountain	Hill (100–200 m)	Low-elevation hill	Medium-elevation hill	Medium-high-elevation hill	High-elevation hill	–
	Mountain with small relief (200–500 m)	Low-elevation mountain with small relief	Medium-elevation mountain with small relief	Medium-elevation mountain and high-elevation mountain with small relief	High-elevation mountain with small relief	–
	Mountain with medium relief (500–1000 m)	Low-elevation mountain with medium relief	Medium-elevation mountain with medium relief	Medium-elevation mountain and high-elevation mountain with medium relief	High-elevation mountain with moderate relief	Extremely high-elevation mountain with medium relief
	Mountain with large relief (1000–2500 m)	–	Medium-elevation mountain with large relief	Medium-elevation mountain and high-elevation mountain with large relief	High-elevation mountain with high relief	Extremely high-elevation mountain with large relief
	Mountain with extremely large relief (>2500 m)	–	–	Medium-elevation mountain and high-elevation mountain with extremely large relief	High-elevation mountain with extremely large relief	Extremely high-elevation mountain with extremely large relief

2.4.2. Geological hazards

The intensity distribution map shows the spatial pattern and the severity of landslide hazards. Based on the Global Landslide Catalog [38], a data set of landslide hazard events in the ancient Silk Road area was compiled, and the dot density of geological hazards was calculated by using the following formula [39]:

$$v_0 = \frac{\sum_{i=1}^{n} v_i \frac{1}{d_i^k}}{\sum_{i=1}^{n} \frac{1}{d_i^k}}, (i = 1, 2 \cdots n) \tag{2}$$

where $v_0$is the hazard density of the estimated point, v_i is the hazard density at the ith sample point, d_i represents the distance between the sample point and the estimated point, and k represents the power of the distance that would significantly affect the estimation results.

2.4.3. Droughts

As one of the most common natural hazards in the world, a drought is characterized by a high frequency, a long duration and a wide range of influence. The standardized precipitation evapotranspiration index (SPEI) was selected as the indicator of drought severity. The SPEI, which considers both precipitation and evapotranspiration, has been used worldwide in various drought-related studies [40,41]. Based on the data from CRU precipitation and potential evapotranspiration, a basic calculation formula of the SPEI for the study area was constructed [42]:

$$F(x) = \left[1 + \left(\frac{\alpha}{x - \gamma}\right)^{\beta}\right]^{-1} \tag{3}$$

$$p = 1 - F(x) \tag{4}$$

$$w = \begin{cases} \sqrt{-2 \ln p} & if \ p \le 0.5 \\ \sqrt{-2 \ln (1 - p)} & if \ p > 0.5 \end{cases} \tag{5}$$

$$SPEI = w - \frac{C_0 + C_1 w + C_2 w^2}{1 + d_1 w + d_2 w^2 + d_3 w^3} \tag{6}$$

where $F(x)$ is the distribution of the probability density based on the different temporal scales of meteorological stations and α, β, and γ refer to the scale, shape and origin parameters of the D values (D values represent the difference between precipitation and potential evapotranspiration) in a range ($\gamma > D < \infty$), respectively. Parameter p has been defined as describing the probability of exceeding a determined D value, which equals $1 - F(x)$. In addition, the value of the parameter w (probability weighted moments (PWMs)) depends on the p value, while C and d are characteristic parameters, and their values are obtained from the literature [42].

2.4.4. Floods

The frequency of flood occurrences is essential to determining the severity of floods. With buffer zones and GIS overlay analysis, the hazard influence center, influence range, duration and mortality of flood events in each state or province were calculated with the following formula:

$$S_{no} = \sum_{i=0}^{n} Count\left(F_i\right) \tag{7}$$

where S_{no} refers to the grade of the flood hazard, F_i refers to the frequency of flooding, and n refers to the total number of samples.

2.4.5. Freezing hazards and ocean hazards

The spatial distribution of freezing hazards is from the Global Land Ice Measurements from Space (GLIMS) data set, which directly describes the location, boundary, area, width, thickness, and elevation of the highest point and the central line of glaciers. The data for the types and distribution of ocean hazards are from NASA's Goddard Space Flight Center, Ocean Biology Processing Group [43], and the data set describes the characteristics of storm surges, tsunamis, coastal erosion, ocean acidification and red tides.

3. Materials and results

3.1. Study site

The ancient Silk Road covers a vast area of the Earth's surface, including Asia, Europe, Africa and Oceania. Moreover, it passes through several different climate types that differ significantly in terms of their precipitation frequency and intensity. In addition, other factors, such as frequent tectonic plate movements, the effects of different elevations and active erosion, are highly conducive to causing various hazards (Fig. 3). Based on the statistical information from the international Emergency Events Database (EM-DAT), from 1990 to 2016, the countries along the ancient Silk Road experienced 78% of the total natural hazards around the world, including 82% of the world's earthquakes, 79% of the world's debris flows and other geological hazards, 78% of the world's floods and 45% of the world's droughts [44]. Due to the frequent occurrence of natural hazards, many limitations and challenges for hazard prevention and reduction are present, including limited budgets, an insufficient awareness of hazard risk prevention, and incomplete early-stage hazard risk assessments [45,46], which consequently threaten the social development, cultural communication and livelihoods along the Silk Road. To effectively manage multiple hazards and undertake targeted risk prevention, it is necessary to identify the types and severities of multiple hazards in a region to promote hazard prevention and mitigation planning.

3.2. Data materials

3.2.1. Natural environments

The terrain elevation and topographic relief distributions along the ancient Silk Road have been compiled (Fig. 4) by using the GIS spatial analysis functions. The landforms along the route have been classified as plains, plateaus, hills, small-relief mountains, medium-relief mountains, large-relief mountains and extremely large-relief mountains, and listed in Table 1.

The frequent occurrence of multiple hazards is closely influenced by geomorphological conditions. Generally, the topography of the ancient Silk Road is dominated by plateaus, mountains and basins, which present a distribution pattern of high in the middle and low in the north and south, with an elevation difference of more than 8000 m. The middle area includes the Himalayas, extends to the northwest, and transitions into the Pamirs, the Iranian Plateau, and the Alps. This region includes countries in southern Asia and western Asia, such as China, India, Pakistan, Iran, and Turkey; countries in southern Europe, such as Italy and Greece; and countries in Africa, such as Egypt, Libya, and Algeria. Notably, these areas coincide with the spatial distributions of earthquakes and geological hazards, which support the determination of the associated hazard boundaries. In contrast, the low-elevation geomorphological areas to the north and south are mainly located on the Eurasian continent, central Africa, and inland Australia. These areas exhibit high spatial consistency with the distributions of floods, droughts and ocean hazards.

Climate zonation plays a significant role in determining the external environmental factors to form natural hazards. The ancient Silk Road spans many climate zones, including tropical, subtropical, temperate, cool climates (Fig. 5), and freezing zones, which creates a large spatial and temporal variation in precipitation and temperatures. In the tropical regions of southeastern and southern Asia, such as Indonesia, Thailand, Bangladesh and India, high-intensity precipitation directly causes floods and ocean hazards and triggers mountain torrents, debris flows, and landslide hazards in geomorphological sensitive areas. Contrary to the tropical areas, in the countries of eastern Asia, such as western China; central and western Asia, such as Kazakhstan, Iran and Yemen; northern Asia, such as Mongolia and Russia; and in other eastern European countries, such as Turkey and Ukraine, precipitation is rare with low intensity; thus, these regions are vulnerable to drought.

3.2.2. Hazard characteristics

According to the data from the Center for Research on the Epidemiology of Disasters [44], the main types of hazards in the ancient Silk Road area include earthquakes, geological hazards, droughts, floods, freezing events and ocean hazards.

- Earthquakes: The ancient Silk Road is located at the junction of the Arabian Plate, the Indian Plate, and the Eurasian Plate. The collision and compression among the plates result in frequent seismic activity and intense tectonic movements (Fig. 6a). According to data from the China Earthquake Networks Center, the Qinghai-Tibet Plateau and its surrounding areas have experienced 18 earthquakes of magnitude 8 or above and more than 100 earthquakes of magnitude 7.0–7.9 since 1900 [62].

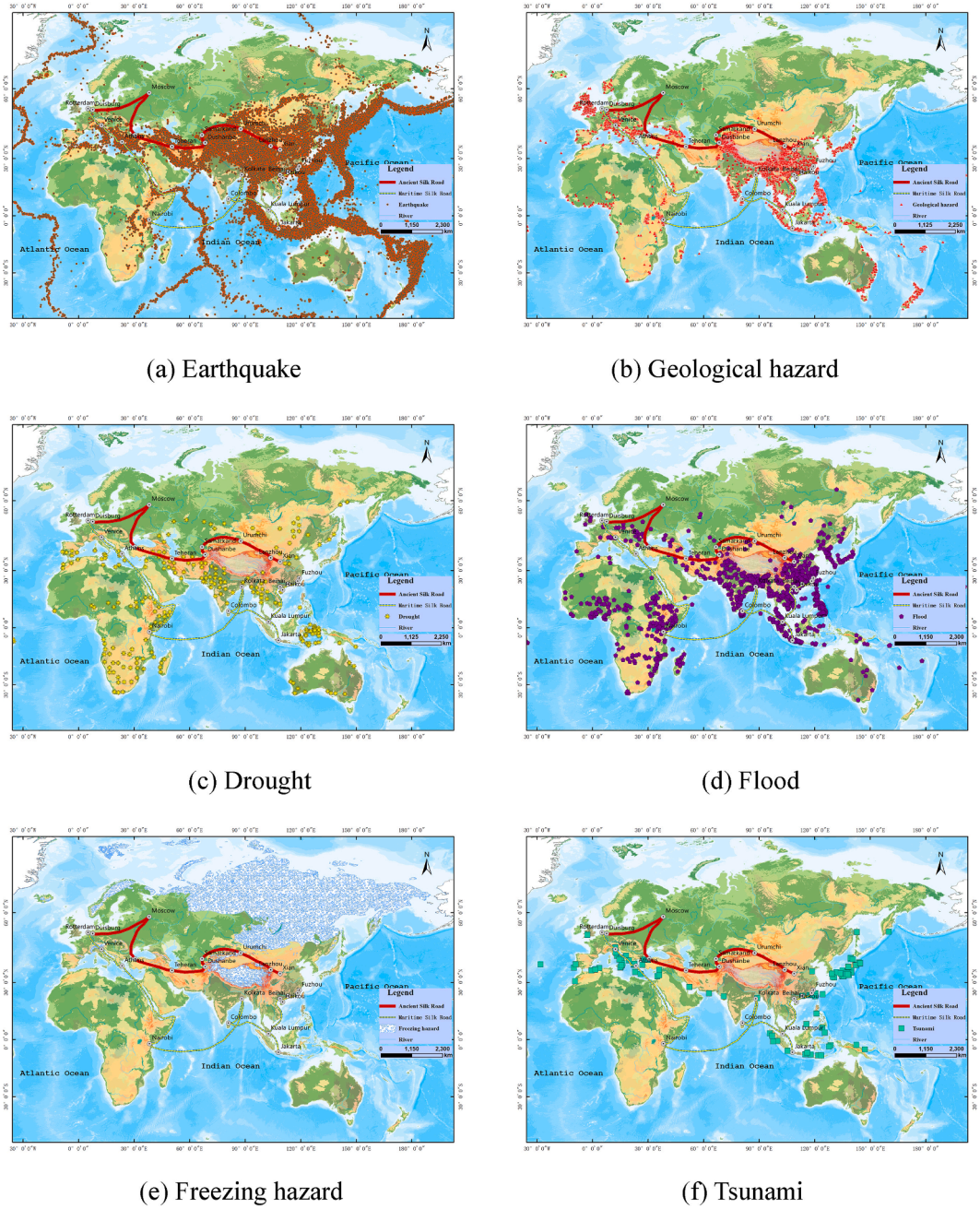

Fig. 3. The spatial distribution of major natural hazards along the ancient Silk Road (Earthquake since 1990, Geological hazard since 2003; Drought since 1961; Flood since 1985; Freezing hazard since 1990; Tsunami since 2000).

- Geological hazards: The catalog of landslide hazards from the Global Landslide Catalog [38] shows a total of 7732 geological hazards occurred in the region from 1922 to 2015. The density distribution map of geological hazards shows that the geological hazards are characterized by an uneven regional distribution and intense local simultaneous occurrences (Fig. 6b).
- Droughts: The average severity distribution of the droughts along the ancient Silk Road (Fig. 6c). Especially in the Sahara Desert of Africa, central Asia, western Asia, Oceania and Russian Siberia, the drought severity is very high. Droughts directly or indirectly affect social and economic development and can disrupt the natural environments necessary for human survival.
- Floods: According to the record of flood events since 1985 [47], the flood occurrence frequency map shows that southwestern China, India, eastern Australia, and other regions have high levels of flood occurrences (Fig. 6d).
- Freezing hazards: According to the data from International Permafrost Association [48], freezing hazards are mainly distributed in high-elevation areas, the cold temperate zone, or the frigid zone along the ancient Silk Road (Fig. 6e).

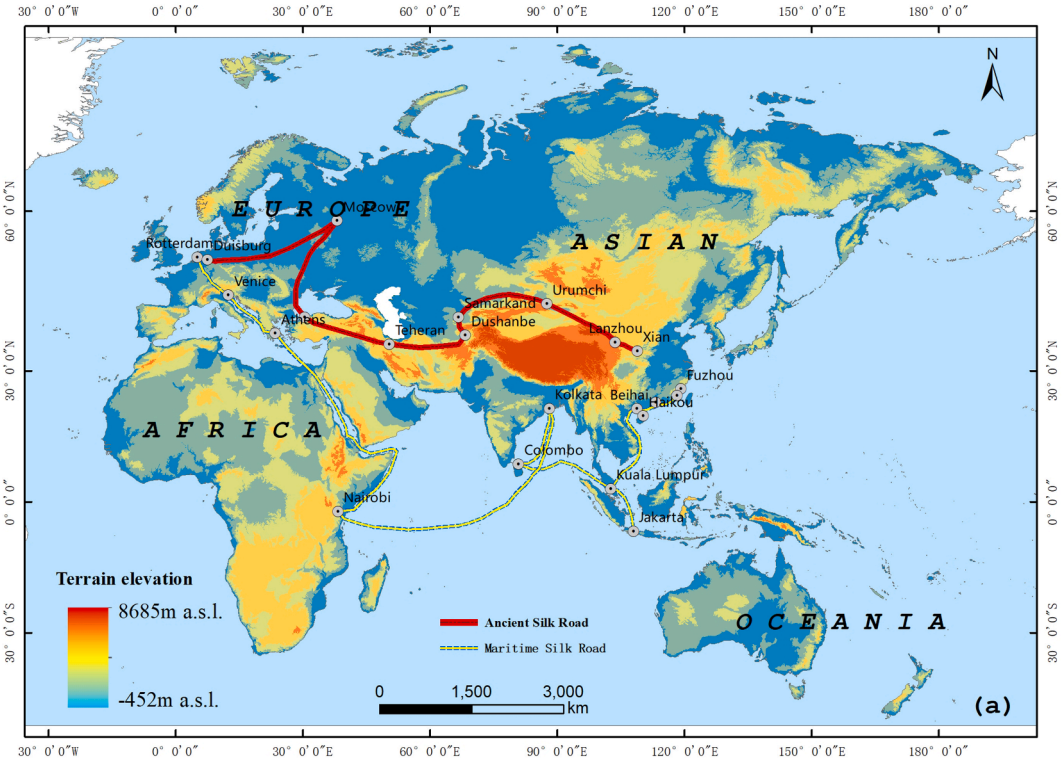
30° 0′ 0″W
0° 0′ 0″
30° 0′ 0″E
60° 0′ 0″E
90° 0′ 0″E
120° 0′ 0″E
150° 0′ 0″E
180° 0′ 0″
60° 0′ 0″N
30° 0′ 0″N
0° 0′ 0″
30° 0′ 0″S
N
EUROPE
ASIAN
AFRICA
OCEANIA
Moscow
Rotterdam
Duisburg
Venice
Athens
Teheran
Samarkand
Dushanbe
Urumchi
Lanzhou
Xian
Fuzhou
Kolkata
Beihai
Haikou
Colombo
Kuala Lumpur
Jakarta
Nairobi
Terrain elevation
8685m a.s.l.
-452m a.s.l.
Ancient Silk Road
Maritime Silk Road
0
1,500
3,000
km
(a)

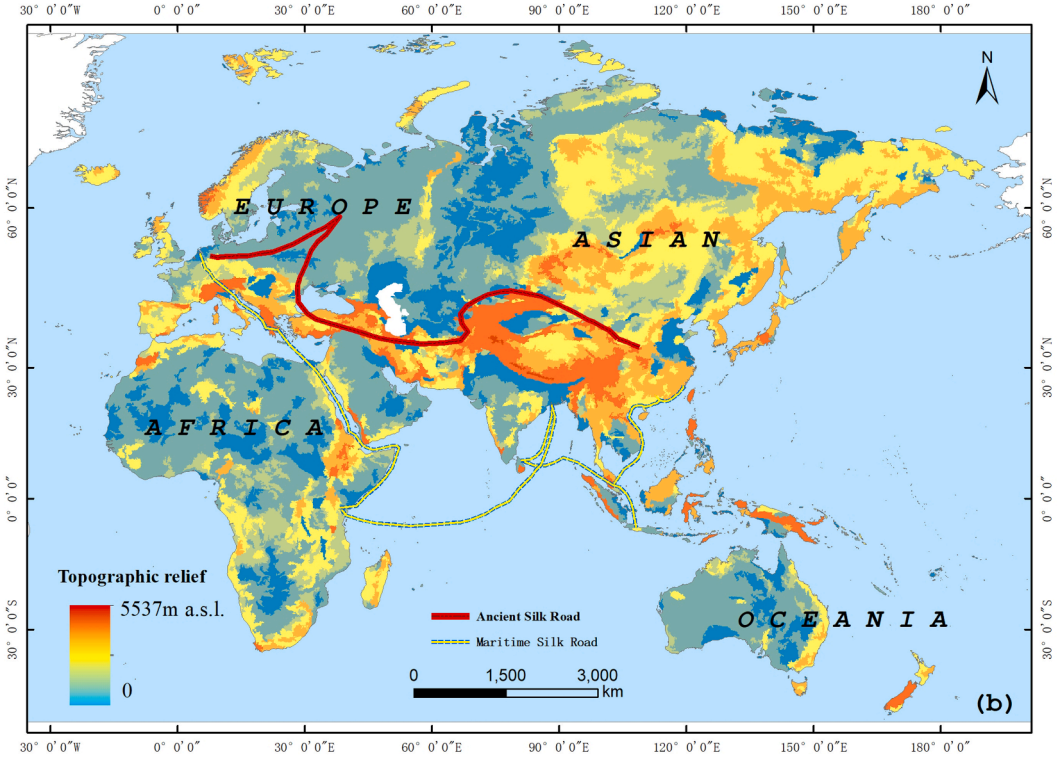
30° 0′ 0″W
0° 0′ 0″
30° 0′ 0″E
60° 0′ 0″E
90° 0′ 0″E
120° 0′ 0″E
150° 0′ 0″E
180° 0′ 0″
60° 0′ 0″N
30° 0′ 0″N
0° 0′ 0″
30° 0′ 0″S
N
EUROPE
ASIAN
AFRICA
OCEANIA
Topographic relief
5537m a.s.l.
0
Ancient Silk Road
Maritime Silk Road
0
1,500
3,000
km
(b)

Fig. 4. The elevation map (a) and topographic relief map (b) of the ancient Silk Road.

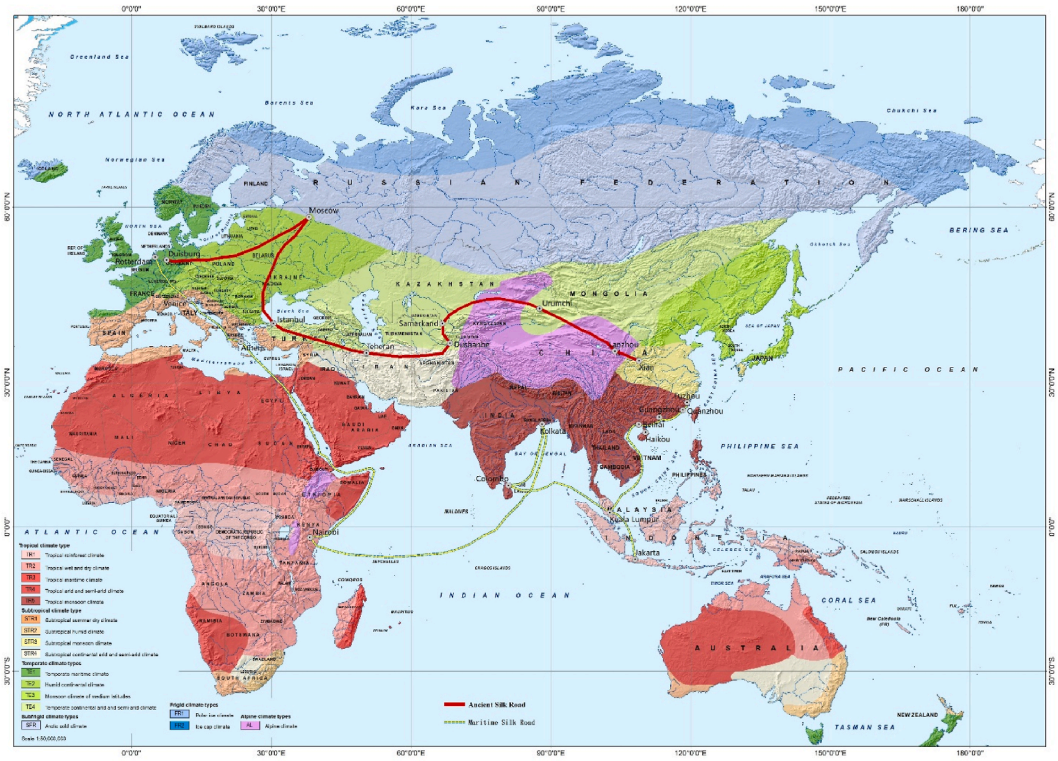

Fig. 5. Climate zonation map of the ancient Silk Road.

- Ocean hazards: Most countries along the ancient Silk Road are affected by ocean hazards, and the main types of ocean hazards include storm surges, tsunamis, coastal erosion, ocean acidification and red tides. The sea level rise caused by climate change will aggravate ocean hazards (Fig. 6f).

3.3. Results

Based on the intensity distribution of each typical type of hazard along the ancient Silk Road and the external hazard-forming environmental conditions (e.g., geomorphology and climate), the presented MIZ method was applied to identify the major hazards and their ranges when a variety of hazards occurred simultaneously within the same region. Controlled by environmental factors such as large geological structures, seismic belts and climatic differentiation, the spatial pattern of natural hazards in the ancient Silk Road area presents an obvious widely scattered distribution of single hazards and a more concentrated distribution of multiple hazards (Fig. 7).

In the ancient Silk Road area, droughts are mainly influenced by the differences between marine and continental climates and the barrier effect imposed by topography. Droughts occur mainly in central Eurasia (northern Asia, central Asia and western Asia), most of the inland areas of Africa (northern Africa and south to north in central Africa), and the inland areas of western Australia. Affected by the spatial and temporal differences in precipitation and by differences between marine and continental climates, floods are mainly distributed in the coastal areas of Eurasia (eastern Asia, southern Asia, southeastern Asia, and western Europe) and along the eastern coast of Africa and the eastern coast of Australia. Freezing hazards are mainly located in the high-elevation area of the Qinghai-Tibet Plateau and the northern part of Eurasia because of the influence of different elevations and solar radiation inputs. Ocean hazards are mainly distributed in the coastal areas and islands of Asia, Africa, and Australia. Under the influence of geological structures and plate movements, the distribution of earthquakes and geological hazards extends from the vicinity of the Himalayas northwest across the Iranian Plateau to the Alps. In addition, because of the differences in climate and topography, there are also clusters of drought and flooding that overlap the spatial distributions of earthquakes and geological hazards.

The statistical results in Table 2 show all types of natural hazards in the ancient Silk Road regions. Accordingly, when travelling along the central route of the ancient Silk Road from east to west, it is highly probable that drought in Central and West Asia, earthquakes and geological hazards on the Iranian Plateau, freezing hazards on the way to Russia, and floods and geological hazards will be experienced before reaching West Europe.

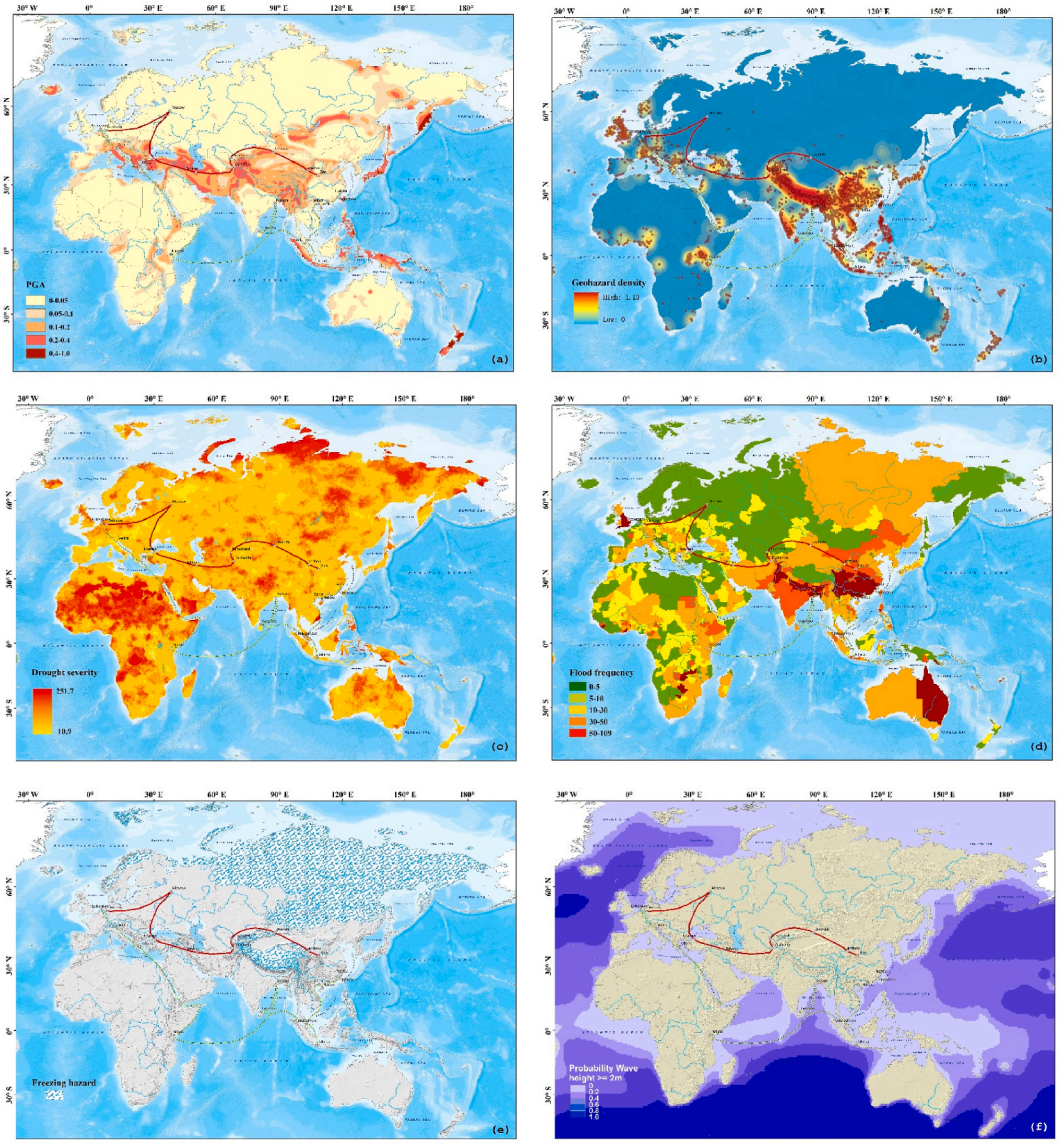

Fig. 6. The intensity distribution of major hazards along the ancient Silk Road. (The figures, in order, show (a) earthquakes, (b) geological hazards, (c) droughts, (d) floods, (e) freezing hazards and (f) ocean hazards).

3.4. Comparison and validation

By using the hazard zoning method developed by Ref. [49]; the severity distributions of earthquakes, geological hazards, droughts, floods, ocean hazards, and freezing hazards overlapped, and the integrated severity was classified into the five levels of very high, high, medium, low, and very low. Then, the severity distribution of the natural hazards (hereafter referred to as "severity zonation" (SZ)) (Fig. 8a) was obtained for the ancient Silk Road. Accordingly, the severity distribution results and the multi-hazard integrated zonation generated by the presented MIZ method (hereafter referred to as "integrated zonation" (IZ) (Fig. 8b) were analyzed by comprehensively comparing their differences from the macro- and microscale perspectives. As an example, South Asia was selected as a typical case study site with complex conditions of hazard formation. In particular, the area of South Asia is affected by activity along geological structures in the Himalayas generated by the relative movement between the Eurasian Plate and the Indian Ocean Plate and by a tropical climate and subtropical plateau climate.

The following observations were made for the entire area of the ancient Silk Road. (1) The SZ map (Fig. 8a) provides information on the intensity distribution in countries along the route. Additionally, the IZ map (Fig. 8b) not only provides zones with the highest hazard severity, but can also identify the types of hazards in the areas where multiple hazards could occur. For example, South Asia is dominated by earthquakes, geological hazards and flood hazards; Southeast Asia mainly suffers from earthquakes, geological hazards and ocean hazards; and the Mediterranean is mainly influenced by earthquakes, geological hazards and flood hazards. (2) Although SZ provides the spatial distribution of hazards on different scales based on the severity characteristics of hazards, IZ can further

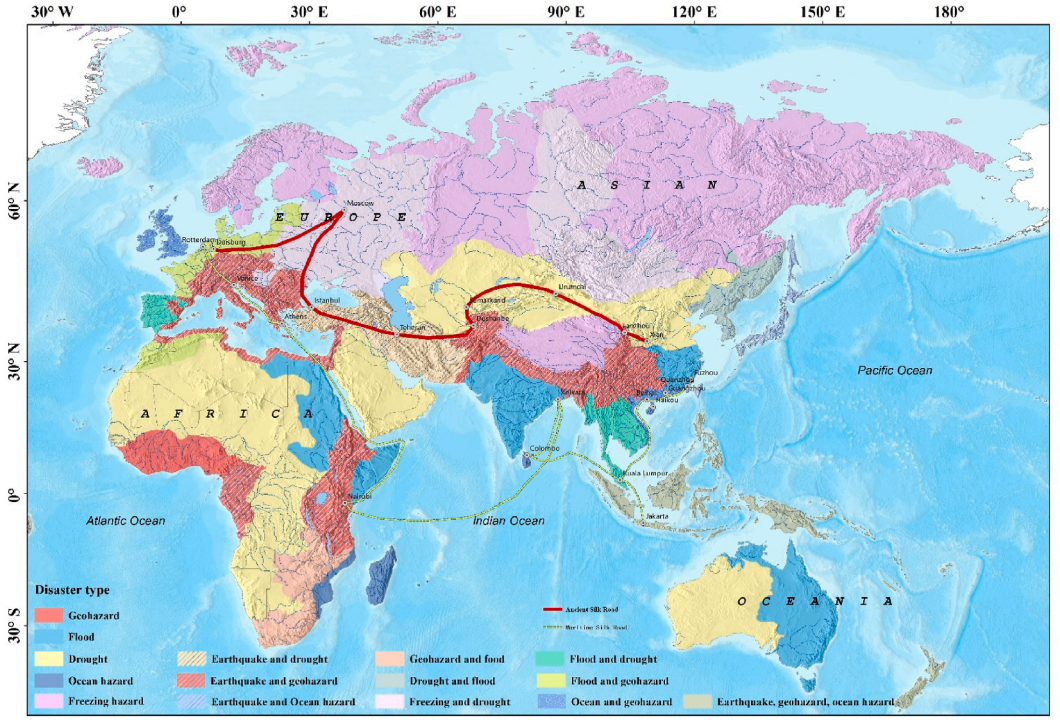

Fig. 7. The integrated zonation of multi-hazards along the ancient Silk Road.

Table 2
The proportion of all types of natural hazards and the associated countries and regions along the ancient Silk Road.

Type of hazard	Area (10, 000 km^2)	Proportion of area	Countries and regions involved
Geographic hazards	249	2.67%	Western Africa such as the Gulf of Guinea
Floods	1075	11.51%	Indian Peninsula in South Asia, eastern plains in Africa, eastern Oceania
Droughts	2923	31.29%	Western and central Asia, Arabian Peninsula, the Sahara Desert, south-central Africa, southeastern Africa, western Asia
Freezing hazards	1599	17.11%	Qinghai-Tibet Plateau in Asia, central Siberia, northern Europe/Scandinavia
Marine hazards	116	1.24%	South China Sea, Sri Lanka, Madagascar, southeastern Africa
Earthquake and geographic hazards	1083	11.60%	The Himalayas, the Mediterranean rim, the Gulf of Guinea in Africa, East Africa Plateau
Earthquake and drought hazards	311	3.32%	Iranian Plateau, Asia Minor Peninsula
Earthquake and ocean hazards	50	0.53%	Southeastern Asia, Japan
Geological and flooding hazards	274	2.93%	East Africa Rift Valley in southeastern Africa
Earthquake, geographic and ocean hazards	324	3.47%	Southeast Asia
Flooding and geographic hazards	177	1.90%	Western Europe, Atlas mountains in Africa
Flooding and drought hazards	192	2.06%	Indochina Peninsula in Southeast Asia, southwestern Europe
Drought and flooding hazards	113	1.21%	East Asia, northeastern plains in Asia
Ocean and geological hazards	73	0.78%	The southern coast of Asia
Freezing and drought hazards	784	8.39%	Mongolian Plateau in central Asia, western Siberian Plain in eastern Asia and eastern European plain

achieve the identification of major hazard types and the corresponding spatial distribution by analyzing the patterns of hazard occurrence and the associated spatial continuity.

The following observations were made for typical regions (Fig. 8c and d). (1) In the SZ map, the severity distributions for different hazards are scattered. For instance, Pakistan is mainly located in very high and high severity zones, which are only hazard intensity zones and hard to provide targeted hazard-oriented support to hazard prevention and reduction in these regions. In the proposed IZ method, earthquakes, geological hazards and droughts are identified as the three main types of hazards. Then, based on a comprehensive analysis of the spatial distribution patterns of the geomorphological conditions and different climate zone including mountain climate, subtropical continental arid and semiarid climate, and tropical monsoon climate, this area can be quantitatively zoned as an earthquake and geological hazard zone, earthquake and drought zone, and flood zone. (2) Similarly, mountain climate and subtropical continental arid and semiarid climate conditions, as well as large-relief geomorphological conditions, are taken into considera-

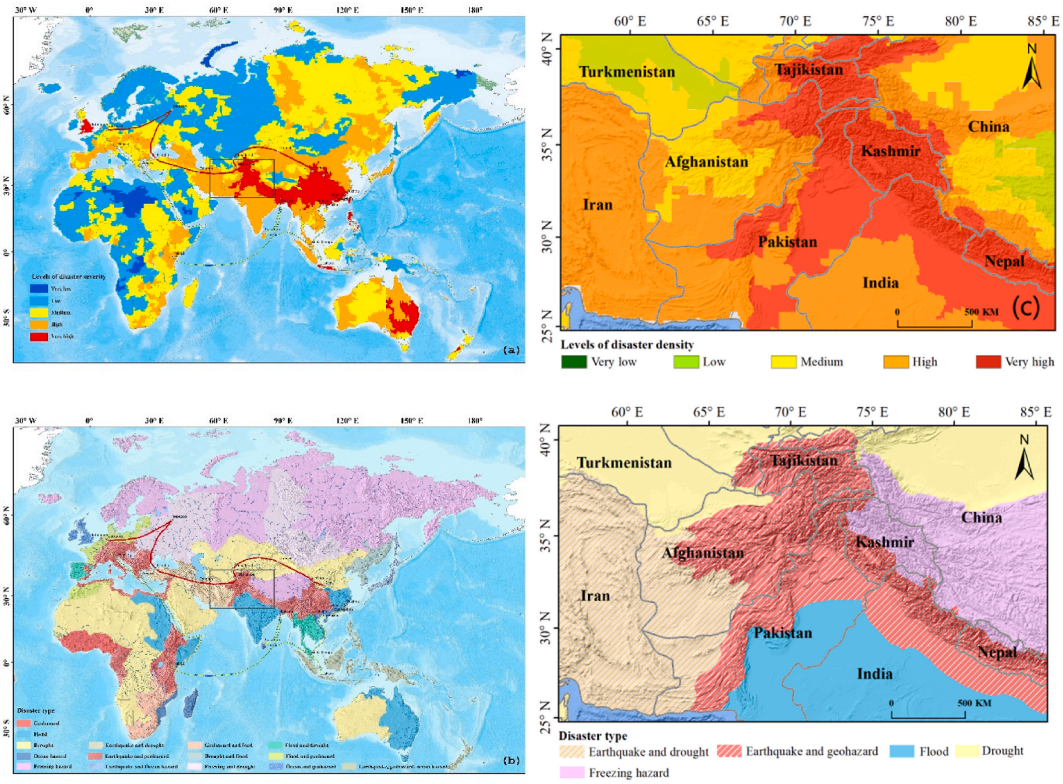

Fig. 8. The comparison between the severity zonation and multi-hazard integrated zonation in typical areas ((a) is the severity zonation map of the ancient Silk Road, (b) is the multi-hazard integrated zonation map of the ancient Silk Road, (c) represents the severity zonation in typical area (South Asia), (d) represents the multi-hazard integrated zonation in typical area (South Asia)).

tion. The areas in Afghanistan classified as having medium and high hazard severity can be further regarded as earthquake and geological hazard zones and earthquake and drought zones through using the MIZ method. (3) By analyzing the geomorphological conditions in the mountains with significant relief, and the subtropical continental arid and semiarid climate zones, Iran's high hazard severity zone can be further classified as an earthquake and drought zone. (4) The Qinghai-Tibet Plateau reaches the level of only a medium hazard severity. However, with the integrated zonation method, the Qinghai-Tibet Plateau can be further identified as an earthquake zone and a geological hazard and freezing hazard zone in accordance with its mountainous climate and extremely high relief.

Accordingly, the proposed MIZ method has identified the major hazard types and has determined the integrated zones for natural hazards in the ancient Silk Road area. Moreover, the resulting maps in accord with the current severity distribution can allow the acquisition of great advantages in allocating relief resources and implementing targeted and uniform measures scientifically, effectively and reasonably.

4. Discussion

The reasonable and quantitative identification of multiple natural hazards is challenging and beyond the generally applied approaches that only focus on single elements in hazard zonation [10,50]. Unlike the current method of severity distribution determination, this study develops a new integrated zoning method to identify the major hazard types and boundaries in muti-hazard areas. This proposed MIZ method improves the current hazard zonation methodology based on the generally applied dual structure approach, which combines only the hazard magnitude and its spatial distribution. According to similarities and the spatial continuity of hazard formation conditions, the zonation patterns of major hazards can be revealed by comprehensively analyzing the spatial distribution of geomorphology and climate. However, due to the limitations of the data and methods in terms of large-scale research, some limitations need to be improved upon. In this study, natural hazards are only described as spatial points or polygons, which ignore detailed characteristics such as landslide scarfs, flood inundation range, regional distribution of PGA and thus influence the susceptibility model performance [25,51]. In addition, this study mainly fucuses on internal hazard mechanism and the external hazard-forming conditions, i.e., the geomorphology and climate zone, but cannot consider the impacts of human activities. The mobility of human beings is an element at risk that produces new challenges for hazard analysis [21]. Therefore, a solution needs to be further developed for integrating the impact of human activities on hazards to assess the variability of hazard distributions under different climatic scenarios.

In this article, the calculated dimensionless severities of different hazards have been used as the basis on which to identify the types of hazards with maximum severity by using a segmented multi-hazard identification function. The multi-hazard integrated zonation based on the hazard formation mechanism intends to quantitatively identify the zonation of natural hazards and provide support for guiding cross-border hazard reduction planning and improving global disaster risk reduction. However, the differences in the maximum severity of different hazards are not considered in the process of integrating the spatial severity distribution. Some studies estimate the average and dispersion of ground motion intensity as well as a set of causal parameters in hazard assessment (e.g., magnitude, source-to-site distance, site conditions) in a particular region [34,52,53]. There is still a lack of uniform quantitative standards to describe the severity dimensions of different hazards [8,45,54,60], and the dimensional analysis of the severity of different hazards presents challenges when considering factors such as the impact of multiple secondary hazards caused by catastrophes via a chain reaction [24,52,55–58]; [7]. Therefore, considering this issue, we assume that the maximum severity of each type of hazard is comparable by the high-technique support. Future research is expected to develop a uniform quantitative standard among different types of hazards to improve integrated hazard zonation.

5. Conclusion

Hazard identification is a critical fundament for disaster risk reduction and may satisfy the needs of hazard mitigation decision-making. In this study, assessment indicators were established to analyze the hazard magnitude, spatial severity distribution and hazard-forming conditions. And a segmented function for multi-hazard identification is proposed to identify multiple hazards simultaneously within a region. In particular, the hazard distribution patterns associated with the climate-tectonic conditions were revealed in the complex natural environment. Accordingly, a new integrated zoning method for multiple natural hazards has been developed by comprehensively analyzing the internal formation mechanisms of hazards and the external hazard-forming environments. A core element of this approach is an internal feedback loop within the system that emphasizes that natural hazard zonation is comprehensive and that multi-hazard integrated zonation should consider the similarities and spatial continuity of hazard formation conditions, i.e., the spatial distribution of geomorphology and climate.

The MIZ method introduces a multi-structure-based analysis and has been applied to a case study of the ancient Silk Road. Based on the hazard-causing mechanism, the elements of external hazard-forming environments referring to the geomorphological characteristics and climatic and the hazard severity and spatial distribution are comprehensively analyzed to determine the possible and reasonable boundaries of multiple hazards. Accordingly, the major types of natural hazards and their extents of hazard-prone zones are determined in the integrated zonation along the ancient Silk Road. The resulting maps of the analysis can better help understand the dominant hazards, which is essential for disaster risk reduction and may serve as pertinent guidance for regional hazard mitigation measures and the rational delineation of infrastructure project layouts in the Silk Road area and beyond.

Author contributions

Qiang Zou, Zhengtao Zhang, and Peng Cui conceived the study. Qiang Zou and Zhengtao Zhang collated base line data and undertook the spatial analysis on multi-disaster integrated zonation. Koert Sijimons improves the Climate zonation map. Giacomo Titti improves the language and structure of manuscript. All authors reviewed the manuscript.

Declaration of competing interest

The authors declare that they have no known competing financial interests or personal relationships that could have appeared to influence the work reported in this paper.

Data availability

Data will be made available on request.

Acknowledgments

This research was supported by the International Partnership Program of Chinese Academy of Sciences (Grant no. 131551KYSB20160002), the Strategic Priority Research Program of Chinese Academy of Sciences (Grant no. XDA20030301) and the Key Research Program of Council of Science and Technology Think Tanks, Chinese Academy of Sciences. The authors thank team members of SiDRR International Research Program.

References

[1] M.D. Frachetti, C.E. Smith, C.M. Traub, T. Williams, Nomadic ecology shaped the highland geography of Asia's Silk Roads, Nature 543 (2017) 193 https://doi.org/10.1038/nature21696, Article.
[2] H.D. Guo, Steps to the digital Silk road, Nature 554 (7690) (2018) 25–27. https://www.ncbi.nlm.nih.gov/pubmed/29388956.
[3] P. Cui, A.D. Regmi, Q. Zou, Y. Lei, X.Q. Chen, D.Q. Cheng, Natural Hazards and Disaster Risk in One Belt One Road Corridors, 4th World Landslide Forum, Ljubljana, Slovenia, EU, 2017, https://doi.org/10.1007/978-3-319-53498-5_131.
[4] Y. Lei, P. Cui, A.D. Regmi, V. Murray, A.P. Pasuto, G. Titti, M. Shafique, D.G.T. Priyadarshana, An international program on Silk road disaster risk reduction-a belt and road initiative (2016-2020), J. Mt. Sci. 15 (7) (2018) 1383–1396. https://link.springer.com/article/10.1007/s11629-018-4842-4.
[5] Z. Gao, The belt and road development strategy and international disaster reduction cooperation (in Chinese), Disaster Reduction China 17 (2015) 1. http://mall.cnki.net/magazine/article/ZGJI201517009.htm.
[6] P. Cui, K.H. Hu, H.Y. Chen, Q. Zou, Risks along the Silk Road Economic Belt owing to natural hazards and construction of major projects, Chin. Sci. Bull. 63

(11) (2018) 989–997, https://doi.org/10.1360/N972017-00867.
[7] Y. Duan, J.N. Xiong, W.M. Cheng, N. Wang, W. He, Y.F. He, J. Liu, G. Yang, J. Wang, J.W. Yang, Assessment and spatiotemporal analysis of global flood vulnerability in 2005-2020, Int. J. Disaster Risk Reduc. 80 (2022) 103201.
[8] E.D. Wickham, D. Bathke, T. Abdel-Monem, T. Bernadt, D. Bulling, L. Pytlik-Zillig, C. Stiles, N. Wall, Conducting a drought-specific THIRA (Threat and Hazard Identification and Risk Assessment): a powerful tool for integrating all-hazard mitigation and drought planning efforts to increase drought mitigation quality, Int. J. Disaster Risk Reduc. 39 (2019) 101227.
[9] G.F. Wieczorek, Preparing a detailed landslide-inventory map for hazard evaluation and reduction, Bull. Assoc. Eng. Geol. 21 (3) (1984) 337–342. https://pubs.geoscienceworld.org/aeg/eeg/article-abstract/xxi/3/337/137205.
[10] S. Pouyan, H.R. Pourghasemi, M. Bordbar, S. Rahmanian, J.J. Clague, A multi-hazard map-based flooding, gully erosion, forest fires, and earthquakes in Iran, Sci. Rep. 11 (1) (2021) 1–19.
[11] F. Nadim, O. Kjekstad, P. Peduzzi, C. Herold, C. Jaedicke, Global landslide and avalanche hotspots, Landslides 3 (2) (2006) 159–173.
[12] S.H. Cannon, J.E. Gartner, M.G. Rupert, J.A. Michael, A.H. Rea, C. Parrett, Predicting the probability and volume of postwildfire debris flows in the intermountain western United States, Geol. Soc. Am. Bull. 122 (2010) 127–144, https://doi.org/10.1130/B26459.1.
[13] Y.N. Wu, P.A. Zhong, Y. Zhang, B. Xu, B. Ma, K. Yan, Integrated flood risk assessment and zonation method: a case study in Huaihe River basin, China, Nat. Hazards 78 (1) (2015) 635–651, https://doi.org/10.1007/s11069-015-1737-3.
[14] C. Huggel, A. Kaab, W. Haeberli, B. Krummenacher, Regional-scale GIS-models for assessment of hazards from glacier lake outbursts: evaluation and application in the Swiss Alps, Nat. Hazards Earth Syst. Sci. 3 (6) (2003) 647–662.
[15] A. Pandey, P.P. Dabral, V.M. Chowdary, N.K. Yadav, Landslide hazard zonation using remote sensing and GIS: a case study of dikrong river basin, Arunachal Pradesh, India, Environ. Geol. 54 (7) (2008) 1517–1529.
[16] M.K. Arora, A.S.D. Gupta, R.P. Gupta, An artificial neural network approach for landslide hazard zonation in the Bhagirathi (Ganga) Valley, Himalayas, Int. J. Rem. Sens. 25 (3) (2004) 559–572, https://doi.org/10.1080/0143116031000156819.
[17] H.J. Qiu, P. Cui, A.D. Regmi, S. Hu, J.Q. Hao, Loess slide susceptibility assessment using frequency ratio model and artificial neural network, Q. J. Eng. Geol. Hydrogeol. 52 (1) (2019) 38–45, https://doi.org/10.1144/qjegh2017-056.
[18] F. Capecchi, P. Focardi, Rainfall and landslides: research into a critical precipitation coefficient in an area of Italy, in: Proc 5th International Symposium on Landslides, 1988 Switzerland. https://ci.nii.ac.jp/naid/10005114855/.
[19] A.K. Saha, R.P. Gupta, M.K. Arora, GIS-Based landslide hazard zonation in the bhagirathi (ganga) valley, Himalayas, Int. J. Rem. Sens. 23 (2) (2002) 357–369, https://doi.org/10.1080/01431160010014260.
[20] A.K. Saha, R.P. Gupta, I. Sarkar, M.K. Arora, E. Csaplovics, An approach for GIS-based statistical landslide susceptibility zonation-with a case study in the Himalayas, Landslides 2 (1) (2005) 61–69, https://doi.org/10.1007/s10346-004-0039-8.
[21] Q. Zou, P. Cui, J. He, Y. Lei, S.S. Li, Regional risk assessment of debris flows in China-An HRU-based approach, Geomorphology 340 (2019) 84–102.
[22] I. Alcántara-Ayala, Geomorphology, natural hazards, vulnerability and prevention of natural disasters in developing countries, Geomorphology 47 (2–4) (2002) 107–124. http://www.sciencedirect.com/science/article/pii/S0169555X02000831.
[23] P. Horton, M. Jaboyedoff, B. Rudaz, M. Zimmermann, Flow-R, a model for susceptibility mapping of debris flows and other gravitational hazards at a regional scale, Nat. Hazards Earth Syst. Sci. (NHESS) & Discussions (NHESSD) 13 (4) (2013) 869–885. http://www.nat-hazards-earth-syst-sci.net/13/869/2013/nhess-13-869-2013.pdf.
[24] P. Cui, Q. Zou, L.Z. Xiang, C. Zeng, Risk assessment of simultaneous debris flows in mountain townships, Prog. Phys. Geogr. 37 (4) (2013) 516–542. https://journals.sagepub.com/doi/abs/10.1177/0309133313491445.
[25] G.D. Bathrellos, H.D. Skilodimou, K. Chousianitis, A.M. Youssef, B. Pradhan, Suitability estimation for urban development using multi-hazard assessment map, Sci. Total Environ. 575 (2017) 119–134.
[26] Y. Battiau-Queney, A tentative classification of paleoweathering formations based on geomorphological criteria, Geomorphology 16 (1) (1996) 87–102, https://doi.org/10.1016/0169-555X(95)00087-L.
[27] W.M. Cheng, C.H. Zhou, Methodology on hierarchical classification of multi-scale digital geomorphology, Prog. Geogr. 33 (1) (2014) 23–33. http://www.progressingeography.com/EN/10.11820/dlkxjz.2014.01.003.
[28] L. Dragut, C. Eisank, T. Strasser, Local variance for multi-scale analysis in geomorphometry, Geomorphology 130 (3–4) (2011) 162–172. https://www.ncbi.nlm.nih.gov/pubmed/21779138.
[29] B.Y. Li, B. Pan, W.M. Cheng, J.F. Han, D.L. Qi, C. Zhu, Research on geomorphological regionalization of China(in Chinese), Acta Geograph. Sin. 68 (3) (2013) 291–306. http://www.geog.com.cn/EN/10.11821/xb201303001.
[30] S. Aggarwal, S.C. Rai, P.K. Thakur, A. Emmer, Inventory and recently increasing GLOF susceptibility of glacial lakes in Sikkim, Eastern Himalaya, Geomorphology 295 (2017) 39–54. http://www.sciencedirect.com/science/article/pii/S0169555X1630887X.
[31] T.M. Andrews, A.W. Delton, R. Kline, High-risk high-reward investments to mitigate climate change, Nat. Clim. Change 8 (10) (2018) 890–894, https://doi.org/10.1038/s41558-018-0266-y.
[32] P. Cui, Y. Lei, Glance at the Silk Road Disaster Risk, Science Press, 2021, pp. 10–18.
[33] E.M. Rathje, N.A. Abrahamson, J.D. Bray, Simplified frequency content estimates of earthquake ground motions, J. Geotech. Geoenviron. Eng. 124 (2) (1998) 150–159.
[34] M. Caprio, B. Tarigan, C.B. Worden, S. Wiemer, D.J. Wald, Ground motion to intensity conversion equations (GMICEs): a global relationship and evaluation of regional dependency, Bull. Seismol. Soc. Am. 105 (3) (2015) 1476–1490.
[35] R. Foulser-Piggott, K. Goda, Ground-motion prediction models for Arias intensity and cumulative absolute velocity for Japanese earthquakes considering single-station sigma and within-event spatial correlation, Bull. Seismol. Soc. Am. 105 (4) (2015) 1903–1918.
[36] K. Chousianitis, V. Del Gaudio, P. Pierri, G.A. Tselentis, Regional ground-motion prediction equations for amplitude-, frequency response-, and duration-based parameters for G reece, Earthq. Eng. Struct. Dynam. 47 (11) (2018) 2252–2274.
[37] K.M. Shedlock, The gshap global seismic hazard map, Int. Geophys. 42 (6) (1999) 1233–1239.
[38] Y. Hong, R. Adler, G. Huffman, Evaluation of the potential of NASA multi-satellite precipitation analysis in global landslide hazard assessment, Geophys. Res. Lett. 15 (2) (2006). https://agupubs.onlinelibrary.wiley.com/doi/full/10.1029/2006GL028010.
[39] G.Y. Lu, D.W. Wong, An adaptive inverse-distance weighting spatial interpolation technique, Comput. Geosci. 34 (9) (2008) 1044–1055.
[40] D.S. Bisht, V. Sridhar, A. Mishra, C. Chatterjee, N.S. Raghuwanshi, Drought characterization over India under projected climate scenario, Int. J. Climatol. 39 (4) (2019) 1889–1911. https://rmets.onlinelibrary.wiley.com/doi/abs/10.1002/joc.5922.
[41] M. Pena-Gallardo, S.M. Vicente-Serrano, J. Hannaford, J. Lorenzo-Lacruz, M. Svoboda, F. Dominguez-Castro, M. Maneta, M. Tomas-Burguera, A. El Kenawy, Complex influences of meteorological drought time-scales on hydrological droughts in natural basins of the contiguous Unites States, J. Hydrol. 568 (2019) 611–625.
[42] S.M. Vicente-Serrano, S. Begueria, J.I. Lopez-Moreno, A multiscalar drought index sensitive to global warming: the standardized precipitation evapotranspiration index, J. Clim. 23 (7) (2010) 1696–1718.
[43] National Aeronautics and Space Administration (NASA), Goddard Space Flight Center, Ocean Biology Processing Group (OBPG), 2016. http://www.opengeospatial.org/resources/data.
[44] Centre for Research on the Epidemiology of Disasters (CRED), International Disaster Database (EM-DAT), 2018. https://www.emdat.be/database.
[45] M.S. Kappes, M. Keiler, K.V. Elverfeldt, T. Glade, Challenges of analyzing multi-hazard risk: a review, Nat. Hazards 64 (2) (2012) 1925–1958. https://link.springer.com/article/10.1007/s11069-012-0294-2.
[46] United Nations International Strategy for Disaster Reduction (UNISDR), Global Assessment Report on Disaster Risk Reduction 2015: *Making Development Sustainable: the Future of Disaster Risk Management*, 2015 Retrieved from Geneva, Switzerland. https://www.preventionweb.net/english/hyogo/gar/2015/en/home/documents.html.
[47] National Aeronautics and Space Administration (NASA), Dartmouth Flood Observatory (DFO), 2017. https://disasters.nasa.gov/programs/dartmouth-flood-

observatory.
[48] National Snow and Ice Data Center (NSIDC), Glacier Database of Global Land Ice Measurements from Space (GLIMS), 2018. http://glims.colorado.edu/glacierdata/.
[49] J.A. Wang, P.J. Shi, Y. Wang, B.J. Li, C.Y. Yang, X.S. Yi, J. Wang, Compilation of city natural disaster Regionalization in China (in Chinese), J. Nat. Disasters 14 (6) (2005) https://doi.org/10.13577/j.jnd.2005.0608, 042-46.
[50] S. De-Angeli, B.D. Malamud, L. Rossi, F.E. Taylor, E. Trasforini, R. Rudari, A multi-hazard framework for spatial-temporal impact analysis, Int. J. Disaster Risk Reduc. 73 (2022) 102829.
[51] K. Papadopoulou-Vrynioti, G.D. Bathrellos, H.D. Skilodimou, G. Kaviris, K. Makropoulos, Karst collapse susceptibility mapping considering peak ground acceleration in a rapidly growing urban area, Eng. Geol. 158 (2013) 77–88.
[52] X. Fan, G. Scaringi, O. Korup, A.J. West, C.J. van Westen, H. Tanyas, R. Huang, Earthquake-induced chains of geologic hazards: patterns, mechanisms, and impacts, Rev. Geophys. 57 (2) (2019) 421–503.
[53] M. Karpouza, K. Chousianitis, G.D. Bathrellos, H.D. Skilodimou, G. Kaviris, A. Antonarakou, Hazard zonation mapping of earthquake-induced secondary effects using spatial multi-criteria analysis, Nat. Hazards 109 (1) (2021) 637–669.
[54] J. Schmidt, I. Matcham, S. Reese, A. King, R. Bell, R. Henderson, G. Smart, J. Cousins, W. Smith, D. Heron, Quantitative multi-risk analysis for natural hazards: a framework for multi-risk modelling, Nat. Hazards 58 (3) (2011) 1169–1192. https://link.springer.com/article/10.1007/s11069-011-9721-z.
[55] K.T. Chang, S.H. Chiang, M.L. Hsu, Modeling typhoon-and earthquake-induced landslides in a mountainous watershed using logistic regression, Geomorphology 89 (3) (2007) 335–347. https://www.sciencedirect.com/science/article/pii/S0169555X07000049.
[56] R.Q. Huang, X.M. Fan, The landslide story, Nat. Geosci. 6 (5) (2013) 325–326, https://doi.org/10.1038/ngeo1806.
[57] J. Qiu, Landslide risks rise up agenda, Nature 511 (2014) 272–273. https://www.nature.com/news/landslide-risks-rise-up-agenda-1.15556.
[58] Q. Zou, G.D.D. Zhou, S.S. Li, C.J. Ouyang, J.X. Tang, Dynamic process analysis and hazard prediction of debris flow in eastern Qinghai-Tibet Plateau area-A case study at ridi gully, Arctic Antarct. Alpine Res. 49 (3) (2017) 373–390.
[59] T. Ghosh, A. Mukhopadhyay, Natural hazard zonation of Bihar (India) using geoinformatics: a schematic approach, Springer Science and Business Media, 2014. https://link.springer.com/book/10.1007/978-3-319-04438-5.
[60] M. Perles-Roselló, F. Cantarero Prados, Problems and challenges in analyzing multiple territorial risks. methodological proposals for multi-hazard mapping, Boletın de la Asociación de Geógrafos Espanoles 52 (2010) 399–404.
[61] K.W. Campbell, Y. Bozorgnia, A ground motion prediction equation for the horizontal component of cumulative absolute velocity (CAV) based on the PEER-NGA strong motion database, Earthquake Spectra 26 (3) (2010) 635–650. https://journals.sagepub.com/doi/abs/10.1193/1.3457158.
[62] Q.D. Deng, S.P. Cheng, J. Ma, P. Du, Seismic activities and earthquake potential in the Tibetan Plateau (in Chinese), Chinese J. Geophys. 57 (7) (2014) 2025–2042, https://doi.org/10.1002/cjg2.20133.